ELSEVIER

Journal of Nuclear Materials 300 (2002) 242–254

journal of nuclear materials

www.elsevier.com/locate/jnucmat

Amorphization and recrystallization of the ABO_3 oxides

A. Meldrum [a,*], L.A. Boatner [b], W.J. Weber [c], R.C. Ewing [d]

[a] *Department of Physics, University of Alberta, Edmonton, AB, Canada T6G 2J1*
[b] *Solid State Division, Oak Ridge National Laboratory, Oak Ridge, TN 37831, USA*
[c] *Fundamental Science Division, Pacific Northwest National Laboratory, Richland, WA 99352, USA*
[d] *Department of Nuclear Engineering and Radiological Sciences, University of Michigan, Ann Arbor, MI 48109-2104, USA*

Received 20 June 2001; accepted 12 October 2001

Abstract

Single crystals of the ABO_3 phases $CaTiO_3$, $SrTiO_3$, $BaTiO_3$, $LiNbO_3$, $KNbO_3$, $LiTaO_3$, and $KTaO_3$ were irradiated by 800 keV Kr^+, Xe^+, or Ne^+ ions over the temperature range from 20 to 1100 K. The critical amorphization temperature, T_c, above which radiation-induced amorphization does not occur varied from approximately ~450 K for the titanate compositions to more than 850 K for the tantalates. While the absolute ranking of increasing critical amorphization temperatures could not be explained by any simple physical parameter associated with the ABO_3 oxides, within each chemical group defined by the B-site cation (i.e., within the titanates, niobates, and tantalates), T_c tends to increase with increasing mass of the A-site cation. T_c was lower for the Ne^+ irradiations as compared to Kr^+, but it was approximately the same for the irradiations with Kr^+ or Xe^+. Thermal recrystallization experiments were performed on the ion-beam-amorphized thin sections in situ in the transmission electron microscope (TEM). In the high vacuum environment of the microscope, the titanates recrystallized epitaxially from the thick areas of the TEM specimens at temperatures of 800–850 K. The niobates and tantalates did not recrystallize epitaxially, but instead, new crystals nucleated and grew in the amorphous region in the temperature range 825–925 K. These new crystallites apparently retain some 'memory' of the original crystal orientation prior to ion-beam amorphization.

1. Introduction

The ABO_3 perovskite-type oxides form a large class of compounds with diverse physical and electronic properties and a variety of crystal structures—the latter often occurring within a given compound at various temperatures as a result of structural phase transitions. The main crystal-chemical requirements for the ideal perovskite structure are that the valence of the A- and B-site cations totals 6+ and that the tolerance factor, t, is between 0.8 and 1.0. Here, $t = (r_A + r_O)/[1.4(r_B + r_O)]$ where r_A, r_B, and r_O are the ionic radii of the A-site cation, the B-site cation, and oxygen, respectively [1]. More than 35 known compounds satisfy these requirements; hence, the perovskite-structure oxides represent a large and important class of phases whose diverse properties provide a unique opportunity for systematically investigating the chemical and structural aspects of radiation-damage and annealing kinetics.

The ideal perovskite structure is cubic Fm3m (Fig. 1), but for tolerance factors lower than 0.9, deformed perovskite structures are favored [2]. In many compounds of this type, a series of displacive phase transitions (rhombohedral → orthorhombic → tetragonal → cubic) occurs sequentially with increasing temperature (see Table 1). The cubic-to-tetragonal transition that takes place on cooling from elevated temperatures may be associated with the formation of a ferroelectric phase and a polarized domain structure. These domain

* Corresponding author. Tel.: +1-780 492 5342; fax: +1-780 492 0714.
E-mail address: ameldrum@ualberta.ca (A. Meldrum).

0022-3115/02/$ - see front matter
PII: S0022-3115(01)00733-4

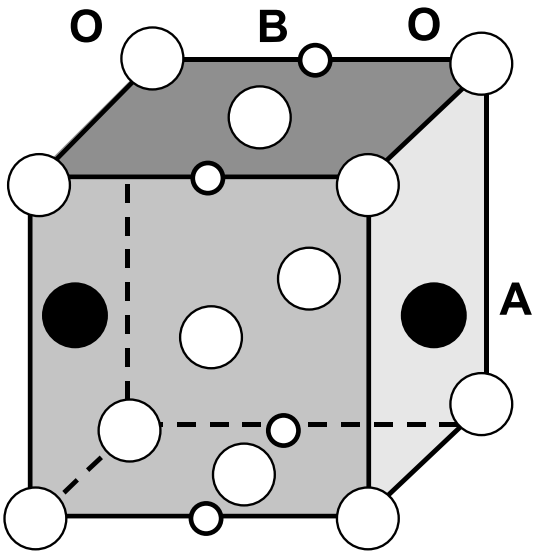

Fig. 1. Ideal cubic perovskite structure, modified from Ref. [1].

structures were investigated in detail using transmission electron microscope (TEM) techniques in a classic early investigation [3] and in subsequent studies (e.g., see Refs. [4–8]).

In addition to their fundamental significance, titanate-based perovskites are also proposed as possible ceramic hosts for the disposal of actinide wastes. $CaTiO_3$ is one of the three main component phases of SYNROC, in which it hosts radioactive Sr, trivalent actinides, and rare-earth elements. In this application, α-decay events will produce damage that accumulates in the perovskite titanate host [9,10] and ultimately compromises its chemical durability. In addition, studies of radiation effects in the ABO_3 oxides are also pertinent to the applied area of the formation of optical waveguides by ion-implantation-induced amorphization (e.g., in the case of $KNbO_3$ and $KTaO_3$ [11–13]).

The present work addresses three primary goals:

1. Determining the chemical/structural parameters and mechanisms that control the kinetics of radiation-induced amorphization and thermal recrystallization in ABO_3 compounds.
2. Determining the effects due to the displacive-radiation spectrum (e.g., incident ion mass and energy) on the competition between the amorphization process and both irradiation-enhanced and thermally induced recrystallization/recovery.
3. Investigating any systematic differences between titanate perovskites with +2, +4 (A,B) cation valencies and the +1, +5 tantalate and niobate compounds.

The effects of ion irradiation were investigated for seven ABO_3 compounds—including three titanates ($CaTiO_3$, $SrTiO_3$, and $BaTiO_3$), two niobates ($LiNbO_3$ and $KNbO_3$) and two tantalates ($LiTaO_3$ and $KTaO_3$). These compounds span a wide range of tolerance factors (0.74–0.94) and crystal structures at room temperature (i.e., rhombohedral to cubic: Table 1).

2. Background

Several previous investigations have focused on the effects of various types of irradiation on oxides with the perovskite structure. $CaTiO_3$ has been widely investigated [14–18] due, in part, to its occurrence in SYNROC. Radiation effects have been studied in $CaTiO_3$ irradiated with 3 MeV Ar^+ ions [19], fast neutrons [20,21], and 1500 keV Kr^+ ions [22–24]. Amorphization of actinide-doped single crystals [25] and of high-purity ion-irradiated crystals [22] occurs at a roughly similar atomic displacement dose (slightly above one displacement per atom [dpa]). In general, $CaTiO_3$ appears to be fairly resistant to the effects of heavy-ion irradiation as compared with other actinide-bearing SYNROC phases

Table 1
Phase transition temperatures, tolerance factors, densities, and melting temperatures for the ABO_3 compounds

Phase	Space group		Transition temperature (K)	t	ρ (g/cm^3)	T_m (K)
	Low T	High T				
$CaTiO_3$	Pcmn	Pm3m	1533	0.81	4.05	2250
$SrTiO_3$	I4/mcm	Pm3m	108	0.86	5.11	2350
$BaTiO_3$	Amm2	P4mm	273	0.93	6.01	1890
	P4mm	Pm3m	393			
$LiNbO_3$	R3c		–	0.74	4.3	1530
$LiTaO_3$	R3c		–	0.77	7.43	1920
$KNbO_3$	R3m	Bmm2	230	0.92	4.61	1350
	Bmm2	P4mm	490			
	P4mm	Pm3m	690			
$KTaO_3$	Pm3m		–	0.94	7.01	1630

such as pyrochlore and zirconolite, and it only becomes amorphous at doses greater than 1 dpa at room temperature [22]. $CaTiO_3$ and $BaTiO_3$ cannot be amorphized by fast neutrons [20] or 4 MeV protons [26], respectively, although displacement damage does occur – mostly due to the formation of oxygen interstitials [26]. The role of the displacive phase transitions in radiation-damage effects in the titanate perovskites may be important, and the polarized ferroelectric phase of $BaTiO_3$ was found to be more susceptible to radiation damage than the non-polarized cubic phase [26]. Interstitial-type dislocation loops tend to preferentially form at the ferroelectric domain walls during electron irradiation in the TEM [27]. Studies of radiation damage in natural perovskite are, however, relatively few [28]. Existing studies suggest that natural uranium- and thorium-bearing $CaTiO_3$ is more resistant to α-decay-induced amorphization than natural pyrochlore or zirconolite, the other principle phases occurring in SYNROC [29–31].

Recrystallization studies have also been carried out on ion-irradiated ABO_3 compounds, and the epitaxial recrystallization rates for ion-beam-amorphized surface layers annealed under similar ambient conditions were determined to decrease generally in the order of: $CaTiO_3$ [32–34], $SrTiO_3$ [35–39], $LiNbO_3$ [35], and $KTaO_3$ [35]. $CaTiO_3$ and $SrTiO_3$ recrystallize epitaxially, but $KTaO_3$ only partially recrystallizes before spontaneous nucleation and growth occur throughout the remaining amorphous layer [35]. The nature of these distinct differences is not well understood and represents a further subject of the present investigation.

3. Experimental procedures

Single crystals of $CaTiO_3$, $BaTiO_3$, and $KNbO_3$ were grown by a flux-based technique, while $SrTiO_3$ was grown by the flame fusion method. The $KTaO_3$ single crystals were grown by solidification from a non-stoichiometric melt, and high-purity single crystals of lithium tantalate and lithium niobate were obtained commercially. The specimens were prepared for in situ ion irradiation in the TEM by gluing 3 mm sections to a slotted nickel TEM grid and then hand polishing to a thickness of ~10 μm. The specimens were subsequently ion milled to perforation at room temperature using 4 keV Ar^+ ions at an incident angle of 20°. Previous experiments have demonstrated that the thin (~2 nm) amorphous surface layer resulting from ion milling has no measurable effect on the amorphization dose [23,40,41], so the specimens were not annealed after ion milling.

The specimens were irradiated at the High-Voltage Electron Microscope (HVEM)-Tandem Facility at Argonne National Laboratory. This facility consisted of a tandem ion accelerator interfaced to a high-voltage electron microscope [42] allowing irradiations to be carried out in situ in the microscope during TEM observation. The samples were irradiated using 800 keV Kr^+ ions at a flux of 1.7×10^{16} ions per m^2/s over a temperature range of 20–1100 K. Irradiations were also carried out using 800 keV Ne^+ and Xe^+ ions. The electron beam was positioned off the sample during most of the irradiation time in order to avoid the potential effects of combined ion and electron irradiations. The amorphization fluence (defined here as the minimum fluence at which the electron-diffraction pattern consists only of diffuse diffraction rings) was monitored by selected-area electron diffraction (see Fig. 2). Diffraction measurements were carried out on regions that were between 80 and 120 nm thick, as estimated by thickness-fringe and convergent-beam measurements. The diffraction measurements were carried out in situ by visual examination of the phosphor screen. The thermocouple that measured the specimen temperature was calibrated by monitoring the disappearance of ferroelectric domain boundaries at 390 and 690 K in unirradiated specimens of $BaTiO_3$ and $KNbO_3$.

The measured amorphization fluence was converted to an equivalent displacement dose measured in dpa using the SRIM Monte Carlo computer code [43] to calculate the average number of displacements per nm per ion from the surface to a depth of 100 nm (the estimated average thickness of the specimens). To obtain a

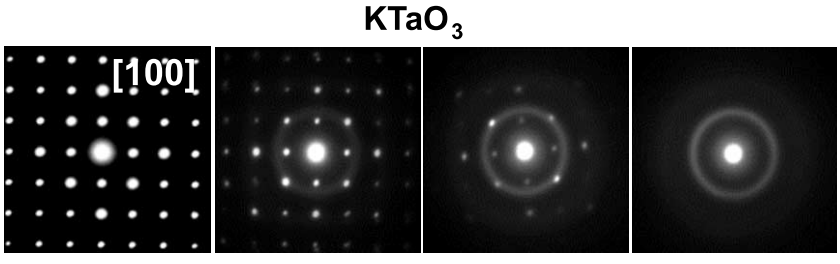

Fig. 2. Sequences of electron-diffraction patterns for $KTaO_3$ irradiated with 800 keV Kr^+ at room temperature. With increasing dose, the electron-diffraction maxima decrease in intensity until, at the amorphization dose (D_c), the diffraction pattern consists only of circular halo characteristic of amorphous material.

relatively accurate conversion factor, a Gaussian distribution function was fit to the SRIM data, and the result was integrated over the 100 nm thickness of the sample [44]. The displacement energies for the perovskites are unknown, and a single representative value of 25 eV was used for all seven phases. The room-temperature experiments were repeated in triplicate, and the variation in the measured amorphization dose was found to be as large as ±12%. In previous experiments [41], the experimental error was found to be as large as ±20%, therefore this value is used in comparing the results for the different phases. The error in the temperature readings was less than ±10°.

Thermal recrystallization experiments were also performed in situ in the high-vacuum environment of the HVEM. The specimens were first irradiated to a fluence twice that required for amorphization. The samples were then heated in 25° intervals and held for 1 min at each temperature. For the purpose of the present experiments, the recrystallization temperature is defined as the temperature at which observable recrystallization occurred within the 1-min time interval. Reproducibility was confirmed by repeating the measurements for $BaTiO_3$, $LiTaO_3$, and $KNbO_3$.

4. Results

4.1. 800 keV Kr^+ irradiation

When irradiated with 800 keV Kr^+ at 20 K, all seven perovskite-type oxides become amorphous between 0.32 dpa ($KNbO_3$) and 0.93 dpa ($SrTiO_3$) (see Fig. 3 and Table 2). These variations are relatively large and are clearly outside the experimental error. The amorphization dose at 20 K is two to three times higher for $SrTiO_3$ and $CaTiO_3$ than for the other five compounds. For the tantalate and niobate compositions, the phases with lithium in the A-site require a slightly higher dose for amorphization than the phases containing potassium.

At higher temperatures, the amorphization dose increased exponentially (Fig. 3). For each compound, a critical temperature, T_c, was defined at which the material cannot be amorphized (i.e., the temperature at which the recovery/recrystallization rate is greater than the rate of radiation-induced damage accumulation, and the amorphization dose increases to infinity). The critical temperature can be estimated from Fig. 3 to increase in the order: $SrTiO_3$, $CaTiO_3$, $BaTiO_3$, $LiNbO_3$, $LiTaO_3$, $KNbO_3$, $KTaO_3$. Several general trends are observed: (a) the critical temperatures are lowest for the titanates, (b) T_c is higher for the potassium-bearing compounds than for those containing lithium, and (c) T_c is higher for the tantalates than for the niobates with the same A-site cation.

The ferroelectric domain structures were straightforward to monitor in the TEM [45]. The presence of these structures had little effect on the measured amorphization dose. Possible effects of the cubic-to-tetragonal phase transition on the amorphization dose were investigated for $SrTiO_3$ and $BaTiO_3$ by performing irradiations at temperatures 20 degrees above and below the transition temperature. In the case of $BaTiO_3$, a slight decrease in amorphization dose was observed at ~380 K, but for $SrTiO_3$ a decrease was not observed. Thus, in contrast to the results for proton irradiation [26], the differences in structure apparently have little effect on the amorphization dose for heavy ions.

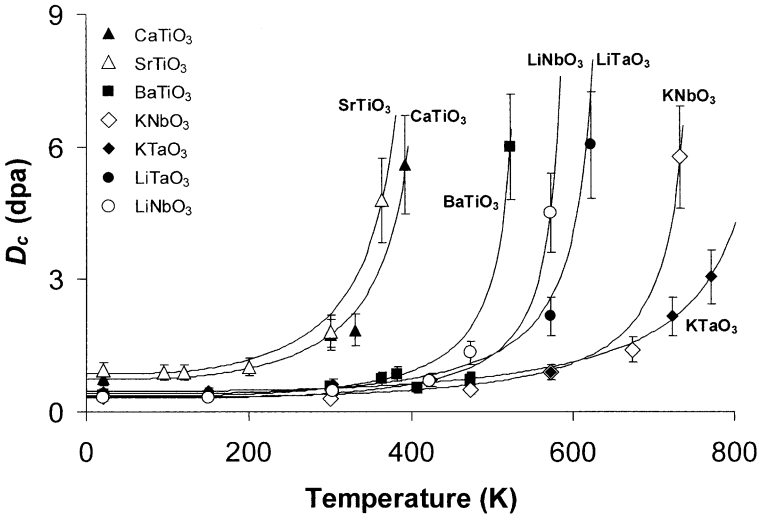

Fig. 3. Temperature dependence of the amorphization dose for irradiation with 800 keV Kr^+ ions. The lines in this and subsequent figures are drawn by a least squares fit to Eq. (1) (see text).

Table 2
Amorphization and annealing data, including electronic and nuclear stopping powers for the various irradiations, D_0 values, critical temperature (T_c), and recrystallization temperature (T_r)

Ion	Compound	dE/dx_n (keV/μm)	dE/dx_e (keV/μm)	D_0 ($\times 10^{18}$ ions/m^2)	D_0 (dpa)	T_c (K)	T_r (K)
800 keV Kr	$CaTiO_3$	1375	1270	3.67	0.75	440	850
	$SrTiO_3$	1439	1378	3.91	0.93	425	800
	$BaTiO_3$	1421	1466	1.46	0.37	550	850
	$BaTiO_3$:Nd	1421	1466	1.53	0.38	590	850
	$LiNbO_3$	1207	1151	1.07	0.32	600	825
	$LiTaO_3$	1464	1063	1.36	0.42	650	925
	$KNbO_3$	1327	1317	1.19	0.35	770	900
	$KTaO_3$	1486	1193	1.53	0.44	880	n.a.
800 keV Xe	$CaTiO_3$	2889	1161	3.40	1.21	440	850
	$SrTiO_3$	3050	1259	2.72	0.97	420	800
800 keV Ne	$CaTiO_3$	64	1282			Not amorphized	
	$SrTiO_3$	66	1367			Not amorphized	
280 keV Ne	$KTaO_3$	70	1200	12.92	0.41	640	n.a.

In the present experiments, insulating specimens are irradiated to relatively high fluences with charged ions. The effects of charge buildup and dissipation may, therefore, affect the measured amorphization dose. Accordingly, a specimen of conducting $BaTiO_3$ was prepared by Nd doping. The resistivity of semiconducting $BaTiO_3$:Nd is nominally 12 orders of magnitude smaller than that of pure undoped $BaTiO_3$. The conducting, Nd-doped specimen was irradiated by 800 keV Kr^+ ions under conditions identical to those used for the pure, insulating $BaTiO_3$, and the amorphization dose was obtained as a function of temperature (Fig. 4). The results are the same within the experimental error, so electrical conductivity and charge dissipation did not have an observable effect on the kinetics of amorphization in the case of $BaTiO_3$.

4.2. Ne^+ and Xe^+ irradiations

The effect of the incident ion mass on the amorphization process was investigated by irradiating specimens of $CaTiO_3$ and $SrTiO_3$ with 800 keV Ne^+ or Xe^+ ions. Neither of these materials amorphized as a result of 800 keV Ne^+ irradiation. In fact, the specimens remained fully crystalline even after receiving a dose of 2 dpa at 20 K. In contrast, both crystals were readily amorphized by 800 keV Xe^+-ion irradiation. The results for the Xe^+ irradiations are shown in Fig. 5 and are compared to the Kr^+ results. The temperature–dose curves are similar over the full range of temperatures. The values of T_c for both phases, estimated from Fig. 5, are approximately 20 degrees higher for the irradiation with Xe^+ than with Kr^+—although this difference is close to the experimental error for this temperature. At low temperatures, the amorphization dose for the Xe^+ and Kr^+ irradiations is nearly identical (see Fig. 5 and Table 2).

In contrast to the cases of $SrTiO_3$ and $CaTiO_3$, $KTaO_3$ is readily amorphized during irradiation with Ne^+ ions. Due to a temporary problem with the accelerator, an incident ion energy of 280 keV was used for $KTaO_3$. The difference in the amount of ballistic energy

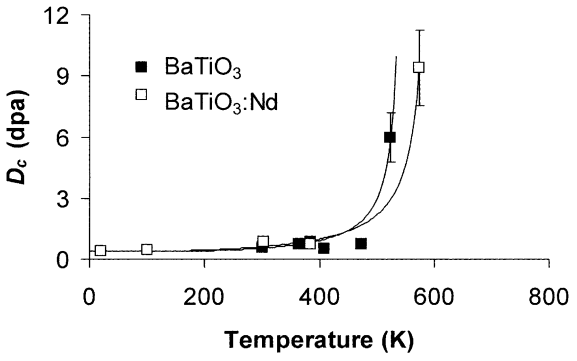

Fig. 4. Temperature dependence of the amorphization dose for insulating and conducting $BaTiO_3$.

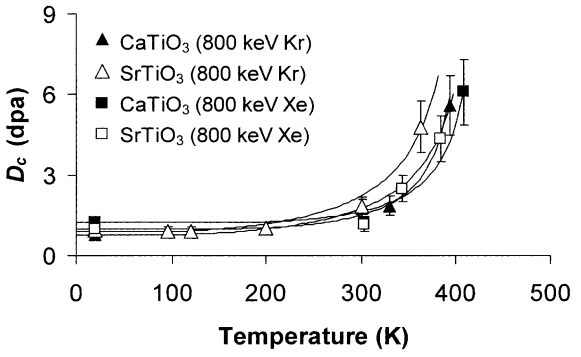

Fig. 5. Temperature dependence of the amorphization dose for $CaTiO_3$ and $SrTiO_3$ irradiated with 800 keV Kr^+ or 800 keV Xe^+ ions.

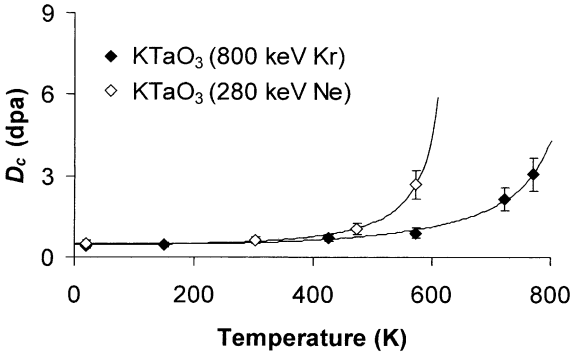

Fig. 6. Temperature dependence of the amorphization dose for $KTaO_3$ irradiated with 800 keV Kr^+ or 280 keV Ne^+ ions.

deposition and concentration of implanted ions is minimal (less than 1% according to SRIM calculations), and in any case, the amorphization dose was normalized in units of dpa. At temperatures below 400 K, the amorphization dose for $KTaO_3$ irradiated with 280 keV Ne^+ or 800 keV Kr^+ ion irradiation was exactly the same, within error (Fig. 6). For the Ne^+ irradiation, T_c is, however, approximately 200 K lower. This significant decrease in the critical temperature with decreasing ion mass was previously observed in $Ca_2La_8(SiO_4)_6O_2$ [46], SiC [47], and in intermetallic alloys [48].

4.3. Thermal recrystallization

One TEM specimen of each compound was irradiated with 800 keV Kr^+ ions at room temperature to a fluence of $2 \times D_c$ and was subsequently heated isochronally in the high-vacuum environment of the TEM in 25 K intervals. The specimen was held at each temperature for 1 min. Here, the temperature for recrystallization was defined to be the temperature at which observable recrystallization occurred within the 1-min time interval. These experiments provide a ranking of the onset of epitaxial recrystallization in a high-vacuum environment for these phases. Several experimental variables could affect the results, including the geometry of the specimen in the electron-transparent regions and specimen thickness variations. Nevertheless, the experiments were repeatable within ±30 K.

In the TEM vacuum environment, the titanates $CaTiO_3$, $SrTiO_3$, and $BaTiO_3$ recrystallized epitaxially from the thick, still-crystalline portions of the TEM specimen that had not been fully penetrated by the ion beam. In all three cases, an amorphous–crystalline boundary progressed toward the thin edges of the specimen, as observed in a previous investigation of the mineral monazite ($CePO_4$) [49], and the resulting microstructure was that of a single crystal. All three titanates recrystallized at similar temperatures, ranging from 800 K for $SrTiO_3$ to 850 K for both $CaTiO_3$ and $BaTiO_3$.

The nature of the thermal recrystallization process in the TEM for the tantalates and niobates was significantly different from that characteristic of the titanates. These differences, as discussed below, are generally consistent with the unusual behavior documented previously for the recrystallization of bulk $LiNbO_3$ and $KTaO_3$ [35].

In the case of $LiNbO_3$, at 825 K in the vacuum environment of the TEM, the amorphous phase recrystallized epitaxially from the thick portions of the TEM foil, but at the same temperature, new crystallites simultaneously nucleated in the thin regions of the specimen. The resulting microstructure consisted of epitaxially recrystallized $LiNbO_3$ bordered by relatively large (200 nm diameter) randomly nucleated crystallites (Fig. 7). Single-crystal electron-diffraction patterns were obtained from the epitaxially recrystallized portion of the specimen (Fig. 7). The distances in reciprocal space correspond to *d*-spacings for monoclinic $LiNb_3O_8$, although zone-axis diffraction simulations produced angles that did not match the experimental patterns by up to several degrees. The recrystallized material could be distorted $LiNb_3O_8$ or, potentially, a new phase. The patterns did not match any low-index zone axis of $LiNbO_3$. The beam spot and selected-area aperture in the HVEM were larger than the precipitates, so single-crystal zone axes from individual particles were not obtained.

For the case of $KNbO_3$, the nucleation and growth of new precipitates occurred at 900 K, resulting in the formation of two separate, microstructurally distinct phases (Fig. 8). Phase I was fine grained (average grain size = 10 nm) and randomly oriented. Phase II occurred as coarse grained (0.3–2 μm) 'microcrystals'. A polycrystalline ring pattern was obtained from Phase I, and single-crystal electron-diffraction patterns were obtained from Phase II. The *d*-spacings obtained by electron diffraction from these two phases are given in Table 3. These phases did not match any phases containing a combination of K, Nb, or O listed in the JCPDS diffraction data file. The ratios of *d*-spacings in Table 3 suggest that the unknown phases do not have cubic symmetry.

The results for $LiTaO_3$ were also unusual in that recrystallization occurred at 925 K—by a random nucleation and growth process (i.e., epitaxial recrystallization did not occur). The resulting 'nanocrystals' were approximately 200 nm in diameter, and surprisingly, they were faceted, aligned, and crystallographically oriented (Fig. 9). This is apparently an initial observation of an oriented phase nucleating from an electron-diffraction-amorphous matrix. The selected-area electron-diffraction pattern from a group of 20 of the crystallites was indistinguishable from that of a single crystal (Fig. 9)

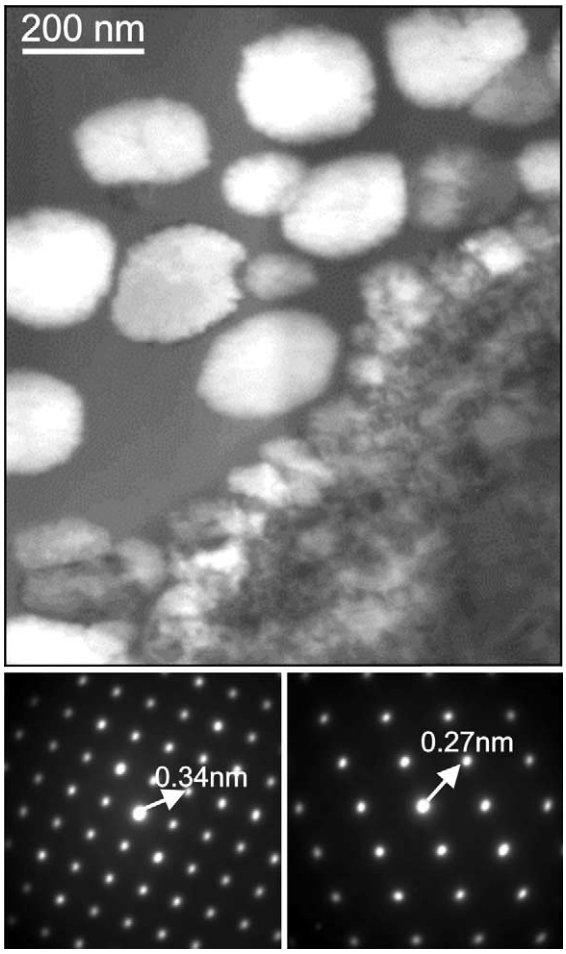

Fig. 7. Thermal recrystallization of ion-beam-amorphized $LiNbO_3$. The specimen recrystallized epitaxially in the bottom right part of the image; however, in the thinnest parts of the specimen, nucleation and growth occurred (upper portion of the image). The selected-area electron-diffraction patterns correspond to the epitaxially recrystallized region. The distances to diffraction maxima are given in real-space units.

and was unambiguously indexable to the [1 1 0] zone axis of 'lithiowodginite' ($LiTa_3O_8$). The original zone-axis orientation of the $LiTaO_3$ was [0 1 2]; however, the equivalence of these two crystal directions should not be assumed because of specimen bending during ion irradiation. The amorphous material remaining between the precipitates contained a high density of ~2-nm-diameter voids or bubbles (Fig. 9). Because of the unusual nature of this microstructure, the experiments were repeated several times with specimens irradiated to a dose of twice D_c. In each case, the results were the same.

The unusual microstructure obtained upon recrystallization of ion-beam-amorphized $LiTaO_3$ warranted further investigation. Accordingly, a bulk sample was prepared by implanting a polished single crystal of

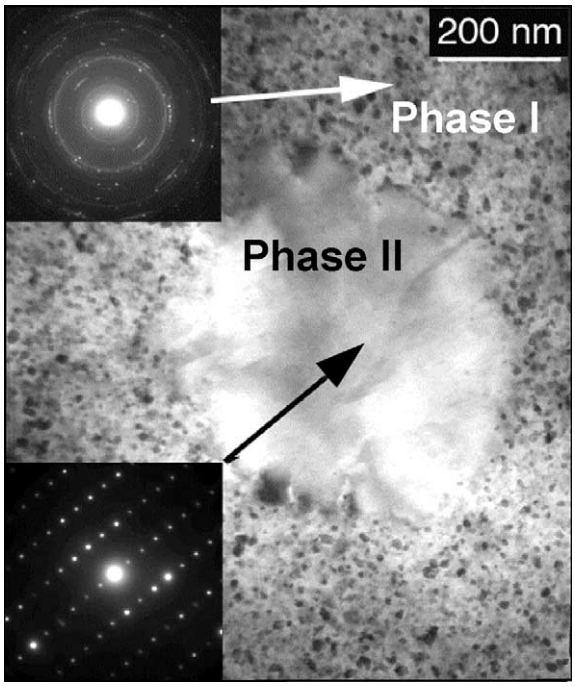

Fig. 8. Thermal recrystallization of ion-beam-amorphized $KNbO_3$. Two microstructurally distinct phases formed, including a fine-grained 'Phase I' and a coarse-grained 'Phase II'. Corresponding *d*-spacings are given in Table 3.

$LaTiO_3$ (identical to the material from which the ion-irradiated TEM specimens were prepared) with 320 keV Xe^{2+} ions at 77 K to a fluence of 5×10^{19} ions/m^2. RBS-channeling results indicated the presence of a layer extending from the surface of the sample to a depth of 150 nm whose backscattered yield matched the random spectrum. A cross-sectional TEM sample was then prepared from the irradiated bulk crystal, and the micrograph in Fig. 10 clearly shows that the sample is amorphous from the surface to a depth of 150 nm. The TEM specimen was then inserted into a double-tilt heating stage, rapidly heated to 800 K, and then heated in 25-degree intervals. Heating continued to 1100 K, and

Table 3
d-spacings (nm) obtained from the electron-diffraction patterns in Fig. 9

Phase I	Phase II
0.64	0.73
0.33	0.39
0.31	0.36
0.27	0.34
0.23	0.27
0.21	⋮
0.19	

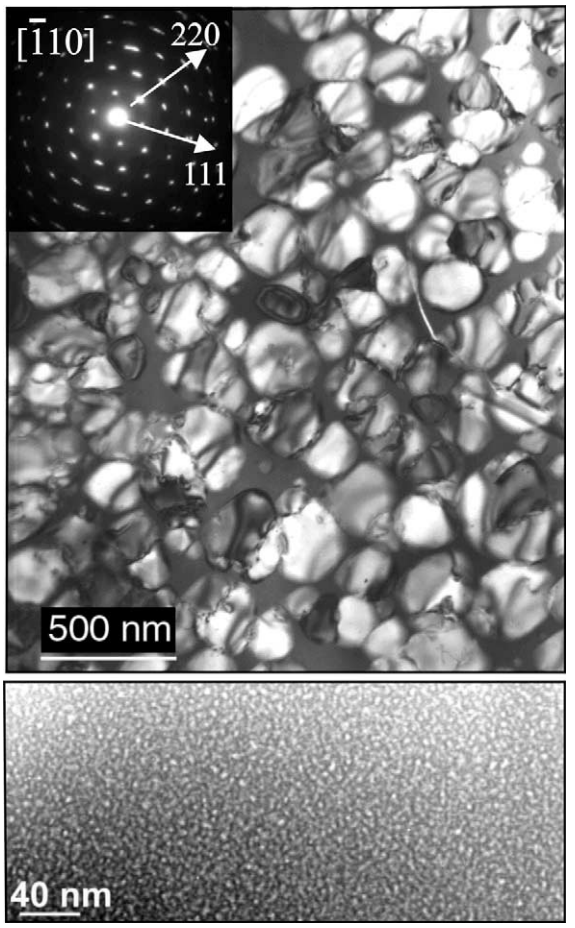

Fig. 9. Thermal recrystallization of ion-beam-amorphized $LiTaO_3$. The resulting crystallites of $LiTa_3O_8$ are faceted and crystallographically aligned, as indicated by the selected-area electron-diffraction pattern obtained from approximately 20 of the particles in the center of the image. Arrows point to higher-order spots for clarity.

the specimen was held at this temperature for 20 min. In contrast to the results for the ion-irradiated TEM specimens described above, no observable crystallization occurred in the high-vacuum environment of the microscope. Higher temperatures were not attempted in the heating stage. The remainder of the bulk implanted specimen was then annealed in an air ambient atmosphere (i.e. in an atmosphere containing water vapor whose concentration was determined by the relative humidity at the time of annealing) at 1400 K for 1 h. A second cross-sectional TEM specimen was then prepared and examined in the TEM. The implanted $LiTaO_3$ was found to have recrystallized epitaxially to the surface of the specimen (Fig. 10). There were few residual defects, and the previous amorphous–crystalline boundary was weakly visible in some areas due to strain con-

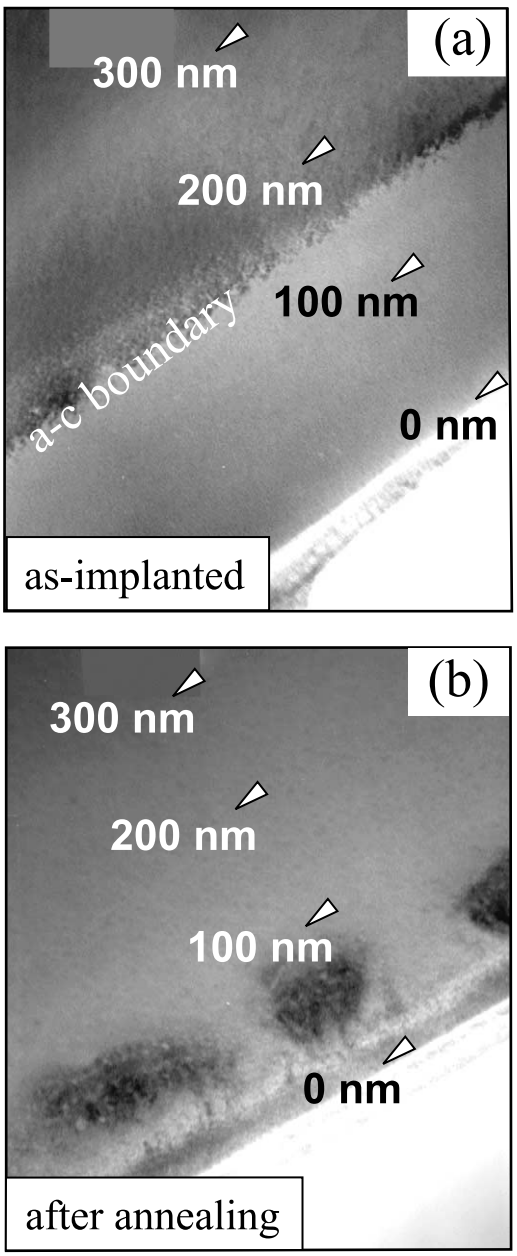

Fig. 10. Cross-sectional image showing epitaxial thermal recrystallization of ion-beam-amorphized $LiTaO_3$: (a) as implanted at 77 K with 320 keV Xe^{2+} ions and (b) the specimen completely recrystallized after annealing in air for 1 h at 1400 K. The regions of dark contrast near the surface in (b) are aggregates of dislocation loops and bubble-like structures.

trast or the presence of isolated dislocation loops. In other areas, regions of high contrast resembling aggregates of dislocations and 'bubble-like' structures were visible closer to the surface (Fig. 10). Thus, the thermal recrystallization of bulk $LaTiO_3$ annealed in an

air/water vapor environment is both qualitatively and quantitatively different than that of thin TEM foils that are both irradiated and annealed in a high-vacuum environment.

In contrast to the titanate compositions, ion-beam-amorphized $KTaO_3$ did not recrystallize at the highest obtainable temperature in the vacuum environment of the electron microscope (1100 K). In fact, no recrystallization was observed after 15 min of continuous observation at this temperature.

5. Discussion

5.1. Amorphization

The amorphization curves shown in Fig. 3 are a result of the competing effects of radiation damage and annealing processes that occur during ion irradiation (e.g., see Ref. [50]). The temperature dependence of the amorphization dose can be obtained using one of several available models [41,50–54]. Since an evaluation of the various models is not an objective here, the curves in Figs. 3–6 were plotted using one of the simplest models [51] that provides a good fit to the data:

$$\ln(1 - D_0/D_c) = \ln(1/\phi\sigma\tau) - E_a/kT \quad (1)$$

Here, E_a is an activation energy for irradiation-enhanced recrystallization, D_0 is the critical amorphization dose at 0 K (extrapolated), ϕ is the ion flux, σ is the amorphization or damage cross-section, τ is a time constant, and k is Boltzmann's constant. The parameters E_a and $\ln(1/\phi\sigma\tau)$ are fit to the experimental data using a standard least-squares technique.

The limitations of this model have recently been discussed in detail, and the activation energies obtained from Eq. (1) are a subject of considerable debate [41,50]. Application of other models, as in the case for the $SrTiO_3$ data [55], yields different activation energies. However, all models yield similar T_c values because a similar general expression is derived for T_c from all models [41,51], which in the case of Eq. (1) is obtained by setting D_c equal to infinity (i.e., $T_c = E_a/k[\ln(1/\phi\sigma\tau)]$). Thus, T_c can be readily determined with confidence from the model fit parameters and verified experimentally.

Calculation of the critical temperature (Table 2) provides a rank order in terms of increasing T_c for 800 keV Kr^+ irradiation: $SrTiO_3$ (425 K), $CaTiO_3$ (440 K), $BaTiO_3$ (550 K), $LiNbO_3$ (600 K), $LiTaO_3$ (650 K), $KNbO_3$ (770 K), and $KTaO_3$ (880 K). No single parameter (including melting temperature, ionicity, tolerance factor, or ratio of electronic-to-nuclear stopping powers) correlates with the critical temperatures of the ABO_3 phases; however, empirical trends can be defined. The critical temperatures increase in the order: titanates, niobates, tantalates, and within each class, there is some tendency for increasing T_c with increasing mass of the A-site cation. A similar ion-mass effect was observed for the ABO_4 orthophosphates [56] and ABO_4 orthosilicates [41,57], olivine [58], spinel [59], and illmenite-type phases [60]; in general, this effect is often observed within groups of isostructural phases.

The amorphization dose can be compared to previous heavy-ion irradiation experiments. Smith et al. [23] found that $CaTiO_3$ could be amorphized by 1500 keV Kr^+ ions at room temperature at a dose of approximately 2.2 dpa – compared to a slightly lower value of 1.8 dpa for 800 keV Kr^+ ions reported here. White et al. [61] reported an amorphization dose of 1.4 dpa at 20 K. This value is almost double the dose obtained at 20 K in the present experiments. The specimen studied by White et al. contained 20% Gd in the Ca site; however, this seems unlikely to cause the factor of two higher dose measured by them. This discrepancy could be attributed to the specimen morphology (White et al.'s perovskite occurred as isolated inclusions embedded in zirconolite); however in the case of zirconolite, Smith et al. also found that the results of White et al. were too high by a factor of two.

Other experimental studies of the amorphization by implantation of bulk single crystals have been reported. For example, Li et al. [62] found that $SrTiO_3$ could not be amorphized by oxygen-ion irradiation at 500 K (above the estimated T_c reported here), but amorphization was readily achieved at room temperature. Weber et al. [55] reported an amorphization dose of 1.0 dpa for $SrTiO_3$ irradiated with 1.0 MeV gold ions at 200 K—identical to the value we obtained for in situ irradiation with 800 keV Kr^+ ions and 800 keV Xe^+ ions at the same temperature. These previous room-temperature heavy-ion-irradiation experiments are generally in good agreement with the room-temperature results of this study.

The effects of irradiation spectrum are demonstrated in Fig. 5 for $CaTiO_3$ and $SrTiO_3$. The amorphization dose curves for 800 keV Kr^+- and Xe^+-ion irradiations are nearly identical, suggesting that the kinetics and mechanisms of amorphization are independent of incident ion mass, at least for heavy ions. Previous work on an intermetallic compound CuTi showed an increase in T_c as one shifts from irradiation with electrons to Ne^+ and from Ne^+ to Kr^+ [48]; however as reported here, the critical temperature was nearly the same for irradiation with Kr^+ and Xe^+. For Kr^+ and Xe^+ irradiation of perovskite, the damage should occur both as widely spaced isolated defects and as high-defect-density regions (or even amorphous zones) within discrete collision cascades and sub-cascades. The equivalence of D_c at low temperature and the slight increase in T_c for irradiation with Xe^+ ions, as compared with Kr^+, implies that the total induced damage is roughly the same for

both ions, but that the damage is more easily recovered at higher temperatures for the Kr^+-ion irradiations. The observed differences are, therefore, attributable to defect geometries and interactions and not to different amounts of damage induced by Xe^+ vs. Kr^+ irradiation.

The titanates did not show any sign of amorphization even after irradiation to 2 dpa at 20 K with 800 keV Ne^+. Clearly, the damage distribution for Ne^+ irradiation will be considerably different than that of the more massive ions. Based on TRIM simulations, most of the irradiation damage is in the form of isolated defects. At temperatures as low as 20 K, defects in $CaTiO_3$ should not be thermally mobile. Any defects produced by the Ne^+ ion irradiation may be activated and driven to recombine through the effects of continuing irradiation, suggesting rapid irradiation-enhanced defect diffusion in the titanates. Electronic energy-loss processes may also assist defect recovery at low temperatures for the Ne^+ irradiation; however, the amount of electronic energy loss is relatively insensitive to ion mass for the ion energies used here (Table 2).

In contrast, $KTaO_3$ was amorphized by 280 keV Ne^+, even at temperatures as high as 570 K. The decrease in ion energy from 800 to 280 keV is not sufficient to account for the large differences between the titanates and $KTaO_3$ (i.e., see Table 2 for a comparison of electronic and nuclear stopping powers for these different ion energies). The relative ease of amorphization with Ne^+ ions implies that isolated defects in $KTaO_3$ do not recombine during irradiation at low temperatures.

In summary: (i) the titanates have lower critical temperatures than their tantalate and niobate analogues, (ii) the displacive phase transitions have little or no effect on the amorphization dose, (iii) within the niobate and tantalate groups, the potassium-bearing composition can be amorphized at higher temperatures than the lithium-bearing ones, (iv) charge dissipation in the substrate does not affect the amorphization dose in $BaTiO_3$, (v) at present, there is no single factor that can be used to predict the relative ranking of the all the perovskite compositions in order of increasing T_c, (vi) T_c depends on the mass of the incident ion, especially for light ions, and (vii) there is a fundamental difference between $KTaO_3$ and the titanates $CaTiO_3$ and $SrTiO_3$ in terms of defect behavior and mobility at low temperature.

5.2. Thermal recrystallization

Previous investigations of the thermal-recrystallization characteristics of ion-beam-amorphized $SrTiO_3$ and $CaTiO_3$ [14,18,32,39] have shed considerable light on the epitaxial-regrowth behavior of these particular compounds. Specifically, this prior work has shown that: (a) For annealing in a water-vapor-containing environment, the epitaxial-regrowth process occurs in two stages (an initial 'induction' stage of relatively slow growth followed by a second 'fast-growth' period) so that the regrowth rate effectively increases with increasing time. For annealing in a dry environment or vacuum, however, the regrowth rate remains constant throughout the entire crystallization process and no second ('fast-regrowth') stage is observed. (b) The overall epitaxial regrowth rate for both ion-beam-amorphized $CaTiO_3$ and $SrTiO_3$ is strongly dependent on the amount of water vapor present in the annealing atmosphere. In fact, water vapor can increase the epitaxial regrowth rate by more than an order of magnitude relative to the rate observed in a dry or vacuum environment. (c) Hydrogen that results from the dissociation of H_2O at the surface of the material is the responsible species leading to the increase in the growth rate. Hydrogen penetrates the amorphous layer to the amorphous/crystalline (a/c) interface and effectively catalyzes the crystallization process by reducing the activation energy – e.g., from a value of 2.14 eV characteristic of the regrowth of $SrTiO_3$ in a high-vacuum environment to a value of 1.02 eV in a water-vapor-containing ambient. Additionally, the absence of oxygen does not affect the regrowth rate. (d) In the case of ion-beam-amorphized $CaTiO_3$, an orthorhombic material, the intrinsic regrowth kinetics (i.e., for anneals in a high-vacuum environment) depend on the crystallographic regrowth direction. (e) In the studies of $CaTiO_3$, it was shown that no thin-section or electron-beam effects occurred in the TEM studies of ion-beam-amorphized single crystals so that the same response was found for amorphous layers on bulk crystals and in TEM thin sections.

In the present work, the ion-beam-amorphized TEM specimens of $CaTiO_3$ and $SrTiO_3$ recrystallized epitaxially from the thick portions of the TEM specimen at 850 and 800 K, respectively, in the high-vacuum environment of the microscope. The 100-degree-higher temperature required for $CaTiO_3$ as compared with previous cross-sectional TEM work [34] may be a function of the recrystallization rate (i.e., observable crystallization in the 1-min time frame requires a crystallization rate greater than $\sim$10 nm/s) and the different geometry of the samples (i.e. in the present case, the amorphous edge of the specimen can be quite far from the thicker, still-crystalline areas). Overall, for $SrTiO_3$ and $CaTiO_3$, the results do agree fairly well with the previous epitaxial recrystallization experiments.

All four niobate and tantalate compositions behave quite differently during recrystallization than do the titanates. In the case of $LiTaO_3$, ion-beam-amorphized TEM specimens recrystallized at 925 K to form discrete, faceted, and coherently aligned particles of $LiTa_3O_8$. This implies the presence of a 'memory' effect in this amorphous material. Two explanations seem plausible: First, the amorphous material may still have a structure that retains a memory of the original crystal structure. An example of this type was documented in the case of

lead pyrophosphate, whose amorphous structure depends on the structure of the original starting material [63]. Second, the electron-diffraction-amorphous phase may not actually be completely 'amorphous'. The electron-diffraction technique is not sensitive to low concentrations of residual crystalline material [64] and, at a dose of $2 \times D_c$, there may be sufficient crystalline nuclei to act as seeds for the recrystallizing phase.

The indexed electron-diffraction patterns of the recrystallized phase were of 'lithiowodginite' ($LiTa_3O_8$). This phase is Li- and O-deficient relative to the original $LiTaO_3$. The lithium that remained unaccounted for must be either in the amorphous matrix around the edges of the particles (Fig. 9) or, owing to its low mass, it may have been ejected from the specimen as a result of the ion irradiation. The 'missing' oxygen may partially account for bubble-like structures observed in the remaining amorphous regions. In direct contrast, the bulk implanted sample showed no evidence of recrystallization in the electron microscope. At least two possible explanations could account for the apparent discrepancy. First, the implanted ion fluence was $\sim 2.5 \times$ higher in the bulk case, so that any residual 'memory' effect in electron-diffraction-amorphous $LiTaO_3$ may have been reduced or eliminated. Second, bulk implantation introduces impurities that concentrate in the amorphized layer, which may also inhibit recrystallization. An effect of this type was documented for natural feldspar, where thermal recrystallization was impeded by the presence of implanted Xe in the amorphous layer [65].

Finally, the bulk-implanted specimen did recrystallize epitaxially to the original $LiTaO_3$ (Fig. 10) when the sample was annealed at 1400 K in an air ambient. The TEM micrograph in Fig. 10(b) shows that at sufficiently high temperatures, the epitaxial recrystallization of the amorphous layer can be completed. Zhang et al. [66] previously found that an ion-beam-amorphized surface layer of $LiTaO_3$ partially recrystallized at temperatures as low as 725 K in a dry oxygen atmosphere, but that the recrystallization front stabilized partway to the surface and no further movement of the amorphous–crystalline boundary was observed. Our specimen was, however, annealed in the presence of water vapor, which is known to considerably enhance the recrystallization rate in several of the perovskite-structure compounds.

Unusual microstructures were also observed in the recrystallization of $LiNbO_3$ and $KNbO_3$. Similarly well-oriented phases did not form; however, recrystallization was not purely epitaxial, and nucleation of new phases did occur. Clear and well-defined electron-diffraction patterns from both recrystallized phases in $KNbO_3$ were obtained; however they could not be unequivocally identified. A large number of stable phases are known in the K–Nb–O system; thus many possible new phases may form during recrystallization. For $LiNbO_3$, the recrystallized material is probably distorted $LiNb_3O_8$. The material did not completely recrystallize and a considerable amount of amorphous material remained between the nucleated crystallites in the thin portion of the TEM specimen, possibly owing to ejection of Li during ion irradiation.

In general, thermal recrystallization of ion-beam-amorphized perovskites is relatively straightforward in the case of the titanites (epitaxial thermal recrystallization), but is a highly complex process for the niobate and tantalite compositions. In these latter phases, epitaxial recrystallization is only a minor process and several compounds may nucleate and grow within the ion-beam amorphized matrix. The low D_c values at low temperatures for the tantalates and niobates, along with the apparent 'memory' of the original crystal structure in the recrystallization experiments may suggest: (1) that the structural differences between the crystalline and the electron-diffraction-amorphous states may be smaller for the tantalates and niobates (i.e., if significant medium-range order is maintained in the amorphous state, then precipitates may nucleate with a preferential crystallographic orientation); and (2) in ion-irradiated thin foils, the observed nucleation and growth recrystallization process has a lower energy barrier than that for epitaxial recrystallization in the case of the tantalates and niobates.

6. Summary

Specimens of $CaTiO_3$, $SrTiO_3$, $BaTiO_3$, $LiNbO_3$, $KNbO_3$, $LiTaO_3$, and $KTaO_3$ were irradiated with 800 keV Ne^+, Kr^+, or Xe^+ ions in situ in a TEM. The estimated critical temperature was found, in general, to increase with increasing mass of the A- or B-site cations. For heavy ions, the susceptibility to amorphization at elevated temperatures depends weakly on the ion mass, although at low temperatures, the amorphization dose is independent of this parameter. This is also true for Ne^+ irradiation of $KTaO_3$ (i.e., T_c was lower but the D_c at low temperatures was the same as for Kr^+); however, $CaTiO_3$ and $SrTiO_3$ could not be amorphized by 800 keV Ne^+ at temperatures as low as 20 K. These results imply a fundamental difference in the amorphization/annealing kinetics between the titanate compositions and $KTaO_3$. This difference was further evident in the thermal recrystallization behavior of the ion-beam-amorphized specimens when annealed in the high-vacuum environment of the TEM. While the titanates recrystallized epitaxially to reform the original single crystal at temperatures of 800–850 K, the niobates and tantalates demonstrated a strong tendency for isolated nucleation and growth that occurred at relatively higher temperatures.

The results demonstrate that titanite-based +2, +4 perovskites do show properties that are more desirable

for nuclear waste applications than their +1, +5 niobate and tantalite analogues. The titanates have higher amorphization doses over a wide range of temperature, are immune to light-ion irradiation, and have lower critical temperatures than the niobate and tantalite perovskites. Thermal recrystallization can occur at lower temperatures and results in epitaxial crystal regrowth; whereas, undesirable new phases may nucleate in radiation-damaged niobium- and tantalum-based perovskites. However, the results also suggest that the incorporation of singly charged impurities (e.g., Na^+) could potentially have adverse effects on the structural response to α-decay-event processes in the titanate perovskites. Further systematic studies will be needed to investigate the effects of impurities substituted into the crystal structure of both $CaTiO_3$ and $SrTiO_3$ in terms of the response to ion irradiation.

Acknowledgements

We thank the staff at the HVEM-Tandem Facility for assistance with the ion irradiations. We particularly thank Ed Ryan for years of patience and his truly caring approach toward facility users, and wish him a long, happy, and productive retirement. A.M. acknowledges support from NSERC, Canada. R.C.E. is supported by BES/DOE (grant # DE-FG02-97ER45656) and L.A.B by the DOE/DMS and the Environmental Management Sciences Program. W.J.W is supported by DOE/BES. Work at ORNL is sponsored by the USDOE under contract DE-AC05-00OR22725 with Oak Ridge National Laboratory (ORNL), managed by UT-Battelle, LLC.

References

[1] F.D. Bloss, Crystallography and Crystal Chemistry, Mineralogical Society of America, Washington, DC, 1994.
[2] K.L. Smith, G.R. Lumpkin, in: J.N. Borland, J.D. Fitzgerald (Eds.), Defects and Processes in the Solid State: Geoscience Applications, Elsevier, Amsterdam, 1993, p. 401.
[3] M. Tanaka, G. Honjo, J. Phys. Soc. Jpn. 19 (1964) 954.
[4] T. Malis, H. Gleiter, J. Appl. Phys. 47 (1976) 5195.
[5] G. King, E.K. Goo, J. Am. Ceram. Soc. 73 (1990) 1534.
[6] B.M. Park, S.J. Chung, J. Am. Ceram. Soc. 77 (1994) 3193.
[7] C.C. Chou, C.M. Wayman, J. Mater. Res. 12 (1997) 457.
[8] O. Popoola, W.M. Kriven, Philos. Mag. Lett. 75 (1997) 1.
[9] A.E. Ringwood, S.E. Kesson, K.D. Reeve, D.M. Levins, E.J. Ramm, in: W. Lutze, R.C. Ewing (Eds.), Radioactive Waste Forms for the Future, North-Holland, Amsterdam, 1988, p. 233.
[10] E.R. Vance, M.W.A. Stewart, G.R. Lumpkin, J. Mater. Sci. 26 (1991) 2694.
[11] T. Bremer, W. Heiland, B. Hellerman, P. Hertel, E. Kratzig, D. Kollewe, Ferroelectr. Lett. 9 (1988) 11.
[12] F.P. Strohkendl, P. Gunter, Ch. Buchal, R. Irmscher, J. Appl. Phys. 69 (1991) 84.
[13] J.Y.C. Wong, L. Zhang, G. Kakarantzas, P.D. Townsend, P.J. Chandler, L.A. Boatner, J. Appl. Phys 71 (1992) 49.
[14] C.W. White, L.A. Boatner, J. Rankin, M.J. Aziz, Mater. Res. Soc. Symp. Proc. 93 (1987) 9.
[15] C.W. White, L.A. Boatner, P.S. Sklad, C.J. McHargue, S.J. Pennycook, M.J. Aziz, G.C. Farlow, J. Rankin, Mater. Res. Soc. Symp. Proc. 74 (1987) 357.
[16] C.W. White, L.A. Boatner, P.S. Sklad, C.J. McHargue, J. Rankin, G.C. Farlow, M.J. Aziz, Nucl. Instrum. Meth. B 32 (1988) 11.
[17] J. Rankin, L.A. Boatner, C.W. White, L.W. Hobbs, Mater. Res. Soc. Symp. Proc. 100 (1988) 453.
[18] J. Rankin, L.W. Hobbs, L.A. Boatner, C.W. White, Nucl. Instrum. Meth. B 32 (1988) 28.
[19] F.G. Karioris, K. Appaji Gowda, L. Cartz, J.C. Labbe, J. Nucl. Mater. 108&109 (1982) 748.
[20] C.J. Ball, R.G. Blake, D.J. Cassidy, J.L. Woolfrey, J. Nucl. Mater. 151 (1988) 151.
[21] K.L. Smith, M.G. Blackford, G.R. Lumpkin, in: I.G. McKinley, C. McCombie (Eds.), Scientific Basis for Nuclear Waste Management XXI, Mater. Res. Soc. Symp. Proc. 506, Materials Research Society, Pittsburgh, PA, 1998, p. 929.
[22] K.L. Smith, N.J. Zaluzec, G.R. Lumpkin, in: I.G. McKinley, C. McCombie (Eds.), Scientific Basis for Nuclear Waste Management XXII, Mater. Res. Soc. Symp. Proc. 506, Materials Research Society, Pittsburgh, PA, 1999, p. 931.
[23] K.L. Smith, N.J. Zaluzec, G.R. Lumpkin, J. Nucl. Mater. 250 (1997) 36.
[24] K.L. Smith, G.R. Lumpkin, M.G. Blackford, E.R. Vance, in: S.J. Zinkle, G.E. Lucas, R.C. Ewing, J.S. Williams (Eds.), Microstructural Processes in Irradiated Materials, Mater. Res. Soc. Symp. Proc. 540, Materials Research Society, Pittsburgh, PA, 1999, p. 323.
[25] H. Mitamura, S. Matsumoto, M.W.A. Stewart, T. Tsuboi, M. Hashimoto, E.R. Vance, K.P. Hart, Y. Togashi, H. Kanazawa, C.J. Ball, T.J. White, J. Am. Ceram. Soc. 77 (1994) 2255.
[26] D.S. Gemmel, R.C. Mikkelson, Phys. Rev. B 6 (1972) 1613.
[27] E.C. Buck, Radiat. Eff. Def. Sol. 133 (1995) 15.
[28] R.C. Ewing, A. Meldrum, L.M. Wang, S.X. Wang, in: S.A.T. Redfern, M.A. Carpenter (Eds.), Transformation Processes in Minerals, vol. 39, Mineralogical Society of America, Washington, DC, 2000.
[29] R.A. Van Konynburg, M.W. Guinan, Nucl. Technol. 60 (1983) 206.
[30] W. Sinclair, A.E. Ringwood, Geochem. J. 15 (1981) 229.
[31] G.R. Lumpkin, M. Collela, K.L. Smith, R.H. Mitchell, A.O. Larsen, in: I.G. McKinley, C. McCombie (Eds.), Scientific Basis for Nuclear Waste Management XXI, Mater. Res. Soc. Symp. Proc. 506, Materials Research Society, Pittsburgh, PA, 1998, p. 207.
[32] J. Rankin, J.C. McCallum, L.A. Boatner, J. Appl. Phys. 78 (1995) 1519.
[33] C.W. White, P.S. Sklad, L.A. Boatner, C.G. Farlow, C.J. McHargue, B.C. Sales, M.J. Aziz, in: H. Kurz, G.L. Olson, J.M. Poate (Eds.), Beam–Solid Interactions and Phase Transformations, Mater. Res. Soc. Symp. Proc. 60, Materials Research Society, Pittsburgh, PA, 1986, p. 337.

[34] J. Rankin, J.C. McCallum, L.A. Boatner, J. Mater. Res. 7 (1992) 717.
[35] C.W. White, C.J. McHargue, P.S. Sklad, L.A. Boatner, C.G. Farlow, Mater. Sci. Rep. 4 (1989) 41.
[36] J.C. McCallum, J. Rankin, C.W. White, L.A. Boatner, Nucl. Instr. Meth. Phys. Res. B 46 (1990) 98.
[37] J.C. McCallum, T.W. Simpson, I.V. Mitchell, J. Rankin, L.A. Boatner, Mater. Res. Soc. Symp. Proc. 235 (1992) 419.
[38] J. Rankin, B.W. Sheldon, L.A. Boatner, J. Mater. Res. 9 (1994) 3113.
[39] T.W. Simpson, I.V. Mitchell, J.C. McCallum, L.A. Boatner, J. Appl. Phys. 76 (1994) 2711.
[40] L.M. Wang, Nucl. Instr. Meth. Phys. Rev. B 141 (1998) 312.
[41] A. Meldrum, L.A. Boatner, S.J. Zinkle, R.C. Ewing, Phys. Rev. B 59 (1999) 3981.
[42] C.W. Allen, E.A. Ryan, in: I.M. Robertson, G.S. Was, L.W. Hobbs, T. Diaz de la Rubia (Eds.), Microstructure Evolution during Irradiation, Mater. Res. Soc. Symp. Proc. 439, Materials Research Society, Pittsburgh, PA, 1997, p. 277.
[43] J.F. Ziegler, SRIM Version 0.05, IBM-Research, Yorktown, NY, 1999.
[44] A. Meldrum, C.W. White, L.A. Boatner, R.C. Ewing, Phys. Rev. B 63 (2001) 104109-1.
[45] A. Meldrum, L.A. Boatner, R.C. Ewing, Nucl. Instrum. Meth. B 141 (1998) 347.
[46] W.J. Weber, L.M. Wang, Nucl. Instrum. Meth. B 91 (1994) 6.
[47] W.J. Weber, L.M. Wang, N.J. Hess, Mater. Sci. Eng. A 253 (1998) 62.
[48] J. Koike, P.R. Okamoto, L.E. Rehn, J. Mater. Res. 4 (1989) 1143.
[49] A. Meldrum, L.A. Boatner, W.J. Weber, R.C. Ewing, Geochim. Cosmochim. Acta 62 (1998) 2509.
[50] W.J. Weber, Nucl. Instrum. Meth. 166 (2000) 98.
[51] W.J. Weber, R.C. Ewing, L.M. Wang, J. Mater. Res. 9 (1994) 688.
[52] K.A. Jackson, J. Mater. Res. 3 (1988) 1218.
[53] G. Carter, M.J. Nobes, J. Mater. Res. 6 (1991) 2103.
[54] V. Heera, T. Henkel, R. Kögler, W. Skorupa, Phys. Rev. B 52 (1995) 15776.
[55] W.J. Weber, W. Jiang, S. Thevuthasan, R.E. Williford, A. Meldrum, L.A. Boatner, in: G. Borstel, A. Krumins, D. Millers (Eds.), Defects and Surface-Induced Effects in Advanced Perovskites, Kluwer Academic, Dordrecht, 2000, p. 317.
[56] A. Meldrum, L.A. Boatner, R.C. Ewing, Phys. Rev. B 56 (1997) 13805.
[57] A. Meldrum, S.J. Zinkle, L.A. Boatner, R.C. Ewing, Nature 395 (1998) 56.
[58] L.M. Wang, W.L. Gong, R.C. Ewing, in: R.J. Culbertson, O.W. Holland, K.S. Jones, K. Maex (Eds.), Materials Synthesis and Processing Using Ion Beams, Mater. Res. Soc. Symp. Proc. 316, Materials Research Society, Pittsburgh, PA, 1994, p. 247.
[59] L.M. Wang, W.L. Gong, N. Bordes, R.C. Ewing, Y. Fei, in: I.M. Robertson, L.E. Rehn, S.J. Zinkle, W.J. Phythian (Eds.), Microstructure of Irradiated Materials, Mater. Res. Soc. Symp. Proc. 373, Materials Research Society, Pittsburgh, PA, 1995, p. 407.
[60] J.N. Mitchell, N. Yu, K.E. Sickafus, M.A. Nastasi, K.J. McClellan, Phil. Mag. 78 (1998) 713.
[61] T.J. White, R.C. Ewing, L.M. Wang, J.S. Forrester, C. Montross, in: T. Murakami, R.C. Ewing (Eds.), Scientific Basis for Nuclear Waste Management XVIII, Mater. Res. Soc. Symp. Proc. 353, Materials Research Society, Pittsburgh, PA, 1995, p. 1413.
[62] Y. Li, R.J. Lui, W-K. Chu, T.J. Tate, Phys. Rev. B 57 (1998) 5668.
[63] B.C. Sales, J.O. Ramey, J.C. McCallum, L.A. Boatner, J. Non-Cryst. Sol. 126 (1990) 179.
[64] M.L. Miller, R.C. Ewing, Ultramicroscopy 48 (1992) 203.
[65] C.L. Melcher, D.S. Burnett, T.A. Tombrello, Proc. Lunar Planet. Sci. 12B (1981) 1725.
[66] Z. Zhang, I.A. Ruskova, W.K. Chu, Nucl. Instrum. Meth. B 136–138 (1998) 404.